CONFERENCE PRE-PRINT

MULTI-SCALE CORE-EDGE INSTABILITIES AND PARTICLE ACCELERATION UNVEILED IN EAST ION TEMPERATURE PEAK DISCHARGE

LIQING XU Institute of plasma physics, CAS Hefei, China Email: lqxu@ipp.cas.cn

BIN, ZHANG, SHIYAO LIN, YAN CHAO, YUQI CHU, KANGNING GENG, YIFENG WANG, KAIYUN CHEN, JINPING QIAN, XIANZU GONG and the EAST Team Institute of plasma physics, CAS Hefei, China

Abstract

Controlling fast particles in tokamaks is crucial for both safe device operation and optimal plasma performance. We report the first observation, on EAST with a fully metallic wall, of a central ion temperature peaking (Ti-peak) regime reaching 9 keV, achieved through the synergistic combination of high-power neutral beam injection (NBI) and argon (Ar) injection. Within this Ti-peak regime, we observe multiple instabilities spanning different scales, including fishbone (FB), long-lived mode (LLM), beta-induced Alfvén eigenmode (BAE), and ion-scale turbulence. Notably, the presence of FB and LLM instabilities is associated with a suppression of ion-scale turbulence and a flattening of the core current density profile. Furthermore, edge fast-ion-driven high-frequency magnetic fluctuations are found to be modulated by an n=0 low-frequency mode excited by core sawtooth crashes, revealing a core-edge coupling mechanism. Ar injection also induces the generation of fast electrons (40–100 keV) in the region around $\rho \approx 0.4$. These findings have immediate implications for future fusion reactors, as the multiscale physics and core-edge coupling dynamics observed here are directly relevant to the management of alpha particles generated by fusion reactions.

1. INTRODUCTION

Achieving high ion temperatures, potentially exceeding 10 keV, is a fundamental requirement for the viability of future fusion reactors. Central to this challenge is the active control of fast particles and the mitigation of ion heat transport, particularly that driven by Ion Temperature Gradient (ITG) turbulence. Observations in devices like DIII-D have revealed that as plasma beta and temperature increase, plasmas often exhibit multi-scale, self-organized behaviour [1]. Core instabilities frequently display global and cross-scale characteristics, with multi-modes appearing even during the initial stages of weak growth. While these multi-scale modes can lead to core fast ion loss, but the flux pumping effect [2-6] induced by cross-scale mode interactions may paradoxically enhance thermal ion confinement by modifying magnetic shear [7-9]. Consequently, addressing ion heating effectively necessitates an integrated approach that considers the complex interplay between energetic particle modes, Magnetohydrodynamic (MHD) instabilities, and micro-turbulence.

Recent experiments suggest that injecting impurities, such as argon (Ar), can suppress ITG turbulence, potentially leading to the formation of Ion Temperature Barrier (ITB) [10]. However, Ar injection also significantly impacts fast ion confinement, offering pathways to mitigate energetic particle loss through mechanisms like destabilizing edge instabilities or modulating plasma flow.

Against this backdrop, the EAST team has recently achieved a central ion temperature peak (Ti-peak) of \sim 9 keV in low-density plasmas heated by Neutral Beam Injection (NBI), utilizing Ar impurity injection. Within this Ti-peak regime, we observed multiple core instabilities, including fishbone (FB), beta-induced Alfvén eigenmodes (BAE), and long-lived modes (LLM), concurrent with a reduction in ion-scale turbulence. Significantly, the injection of Ar impurities also led to a pronounced increase in fast electron production near $\rho\sim$ 0.4. Furthermore, we found that the loss of fast ions could be reduced through the interplay between edge high-frequency magnetic instabilities and n=0 core modes triggered by sawtooth crashes in the Ti-ITB dithering phase. These observations reveal a novel physical mechanism governing fast particle energy exchange under low-collisionality conditions and provide crucial insights into core-edge coupling dynamics, holding promise for addressing similar challenges in future fusion reactors.

2. MULTI-SCALE INSTABILITIES IN THE CORE REGION

An enduring question for axisymmetric magnetically confined plasmas with robust toroidal fields, such as tokamaks and spherical tori, has been the potential existence of coherent nonlinear MHD instabilities featuring multiple toroidal mode numbers at modest amplitudes. This question has now been affirmatively answered. Within the tokamak ITB region, where magnetic shear is notably weak, a persistent LLM mode or a harmonically predominant fishbone mode is consistently observed. SXR diagnostics offer a detailed spatial visualization of these FB and LLM modes [11, 12]. Figure 1 provided the instability information in shot #136377. Two Mirnov coil sets (with signal names khp6t/khp7t/khp8t and lhp6t/lhp7t/lhp8t), which are located at the same poloidal position but separated toroidally by 22.5 degrees and have a sampling rate of 1 MHz, were used to calculate the toroidal mode number of the magnetic perturbation. The toroidal mode number is determined by dividing the phase difference of the mode, within the frequency band of interest, by the corresponding toroidal angle difference (~22.5 degrees). Three modes have been identified, this first mode is fishbone driven by NBI beams [20, 21], with n=1 to n=3. A second modes is BAEs with n=5-7, which is prior to fishbone and is driven by fast particle [21-23]. The last one is LLM [24], with n=1 to n>18. The mode spatial structure of fishbone with n=1 and n=2 is shown in (a) and (b) of Figure 1. A zoomed view of frequency spectrum of LLM measured by core SXR has been shown in (c) of Figure 1. Despite variations in plasma beta, the mode closely resembles the Alfvén ion temperature gradient mode observed in DIII-D when examining the frequency spectrum. The observation of multi-harmonic instabilities in the low β core of EAST suggests that their excitation is more sensitive to the core ion temperature gradient and a near-zero magnetic shear configuration than to the absolute magnitude of the β value. The reconstructed safety factor profile, as confirmed by POINT+EFIT analysis, verifies the flatness in the vicinity of the q=1 surface [11].

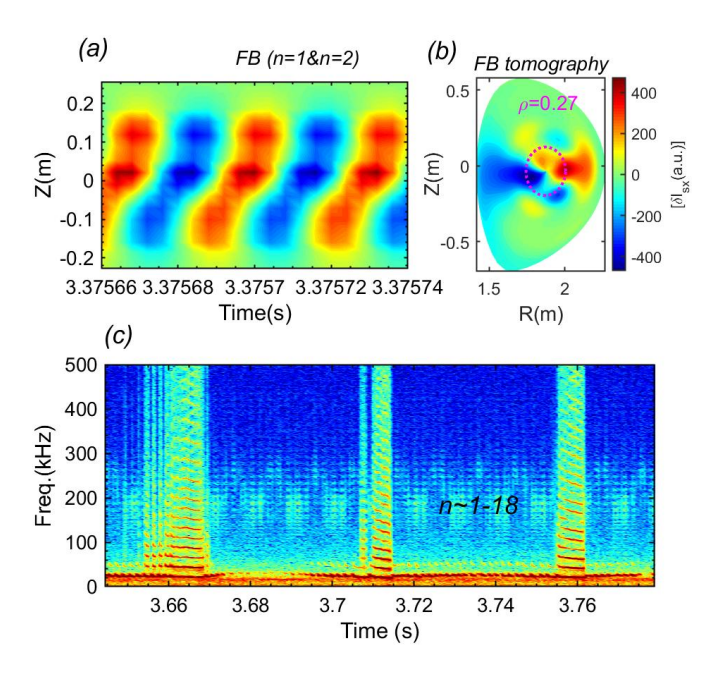


Fig. 1 FB with n=1 and n=2 observed by SXR diagnostic, with non-local transport characters (a) the time-space SXR evolution of FB, (b) tomographic reconstruction of FB, non-local perturbation peaks at 0.27 radius, (c) multiscale mode appearance periodically after FB with a large amplitude. The mode numbers from m/n=1/1 to m/n>18/18. The frequency from 25 kHz to > 400 kHz. In contrast with the previous claim of multiscale mode only in high $\beta_N > 2.5$ and high confinement $H_{98} > 2.5$ discharge in DIII-D, the observed multiscale mode in EAST in low $\beta_N \sim 1.0$ L mode.

In experiment #136377, turbulent data were not adequately available, so we conducted a study on the interaction between macroscopic instabilities and ion-scale turbulence using the #136326 shot, which had comparable discharge parameters. As illustrated, the amplitude of ion-scale turbulence gradually intensified, accompanying with FB and LLM (Fig.2).

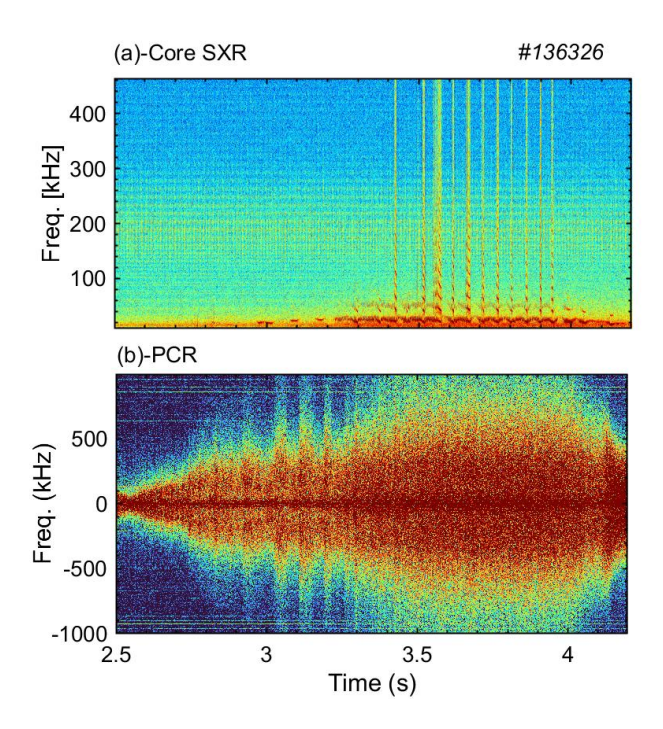


Fig.2 Core turbulence and macroscopic instabilities in shot #136326 with Ti~6 keV. (a) MHD in SXR (b) turbulence measured by poloidal coherent reflectometry [25].

Figure 3 reveals that high-frequency ion-scale turbulence (>200 kHz) was significantly suppressed during the FB bursting phase. This suggests that effectively mitigating such turbulence is key to increasing the central Ti.

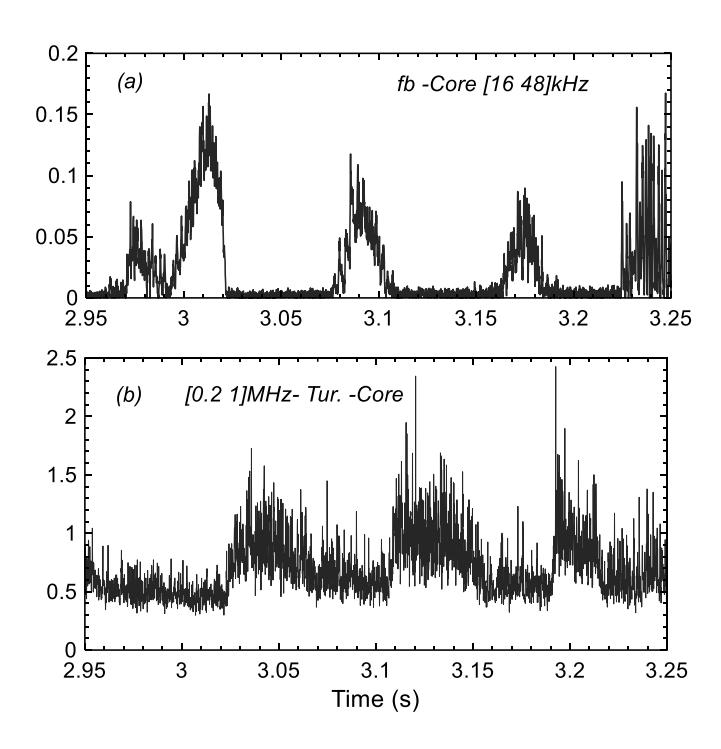


Fig.3 Detailed Analysis of Fast Particle Burst–Turbulence Interaction. (a) Temporal evolution of FB amplitude. (b) Turbulence characteristics in the frequency range [0.2–1] MHz.

3. MODULATION OF CORE CURRENT BY OFF-AXIS LLM

Flux-pumping is understood to play a significant role in the self-organization of the current profile within hybrid scenarios. This mechanism can be triggered by turbulence or MHD-driven magnetic reconnection events, with the focus of this paper being on the latter. The effects of flux-pumping can be observed through various phenomena, including the acceleration of nonthermal particles or the induction of turbulence. Figure 4 depicts a classic instance of flux-pumping driven by the off-axis LLM mode. Form Fig.4 (b), the LLM located near R~2.05m, is not the axis of magnetic surface (Raxis ~1.98 m). A negative current is generated when the amplitude of the MHD mode exceeds a critical value. This negative current within the plasma core inherently results in an increase in q0, which undesirably expands the core current profile and flattens the safety factor (q) profile in the core region. The induced current anomaly spreads inward and broadens the core current distribution in less 1 ms, which is much shorter than the current diffusion time scale. Additionally, the reduction in core magnetic shear leads to a significant reduce of high-frequency turbulence with frequencies ranging from 0.2 to 1 MHz.

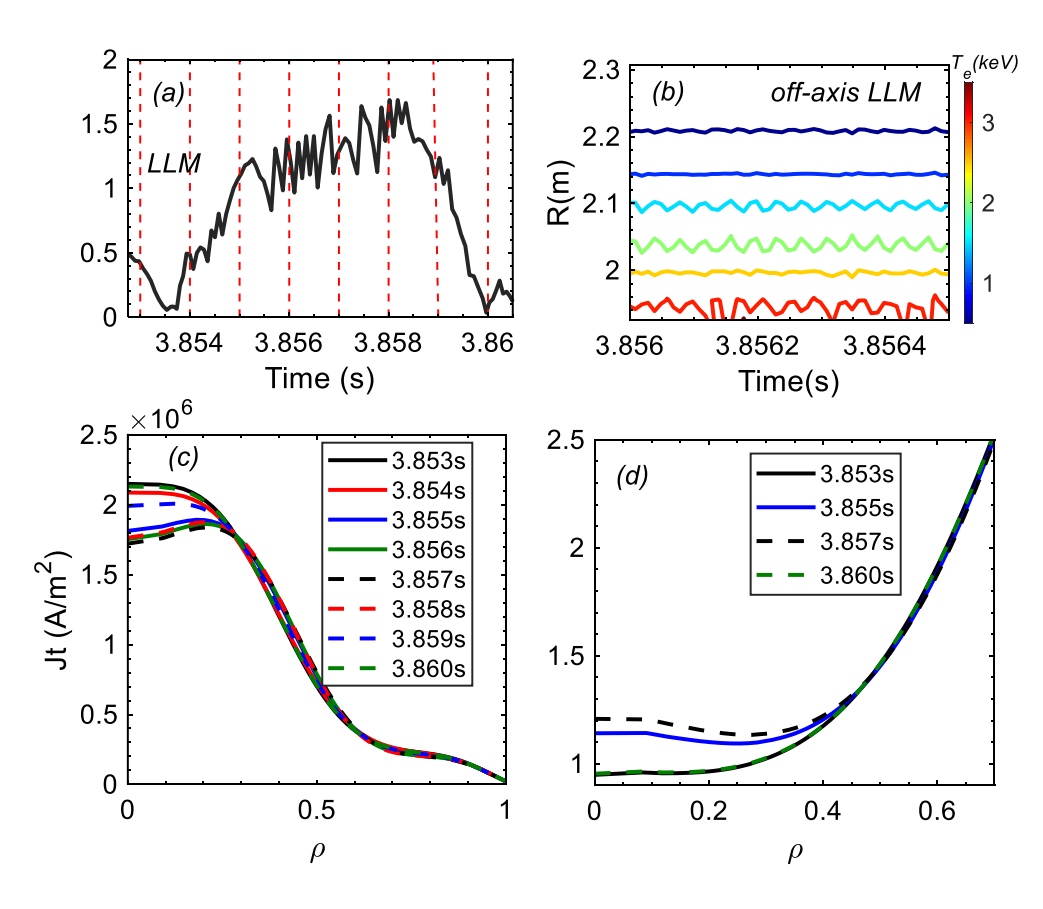


Fig.4 Flux pumping caused by LLM in Ti-ITB region. (a) evolution of amplitude of LLM mode (b) current density J and (c) safety factor q

4. DGE INSTABILITY MODULATION BY CORE SAWTOOTH DRIVEN N=0 MODE IN TI-ITB DITHERING PHASE

In a subset of discharges (#133469), a dithering phase of the Ti-ITB is observed prior to its stable formation. This dithering phase is characterized not only by sawtooth crashes but also by the presence of a low-frequency n=0 mode, as illustrated in Fig. 5 (a). The n=0 mode oscillates at approximately 1.5 kHz. Its activity modulates the edge high-frequency magnetic fluctuations, which exhibit a relatively broad spectrum from 350 kHz to 450 kHz, peaking around 370 kHz. This core-to-edge modulation effect is further corroborated by divertor probe measurements (Fig. 5 (b) and (c)). This phenomenon serves as a typical example of core-edge coupling mediated

by fast ion dynamics, with the perturbation propagating from the core to the edge in roughly 0.2 ms (Fig. 5 (c)). Significantly, the observed modulation of fast ion losses during this ITB-dithering phase underscores the critical role of fast ion confinement in both the formation of the Ti-ITB and the subsequent bursting behavior observed in the core.

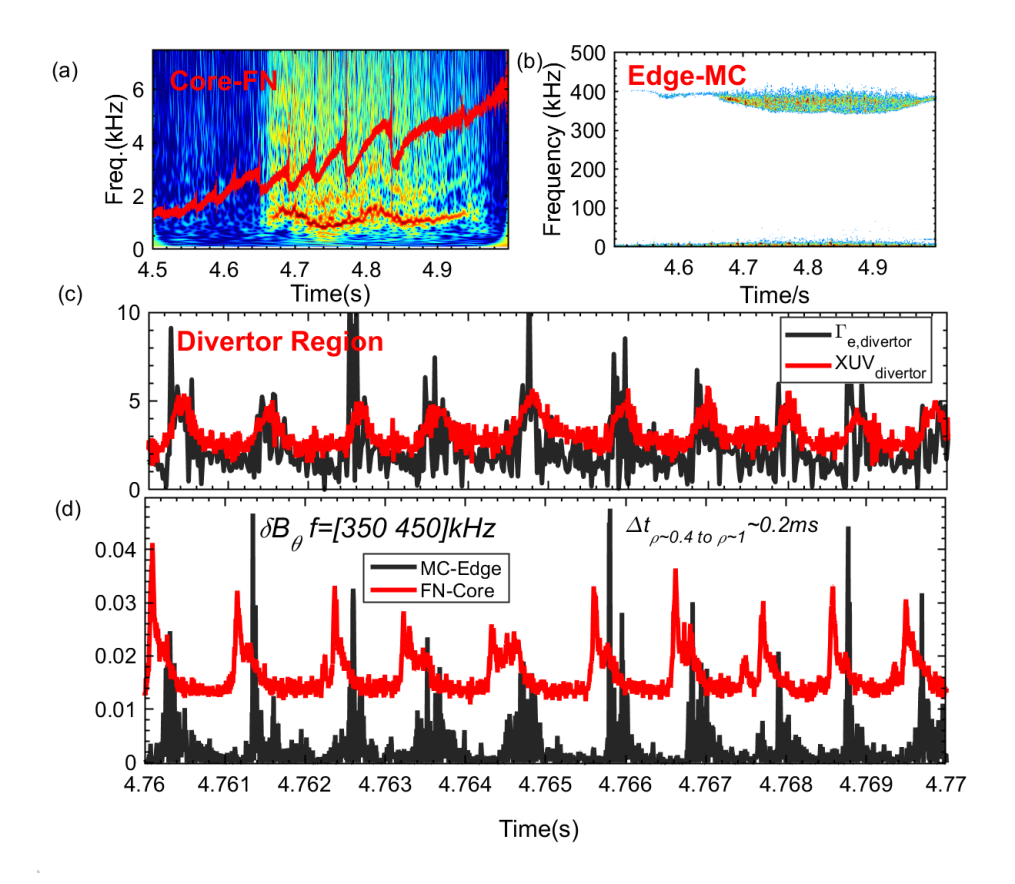


Fig.5 Core-Edge Coupling @ shot#133469: Modulation of Edge Fast Ion Instabilities by the n=0 Mode. (a) Core fast neutron (FN) flux spectrogram [26] with overlaid Core-SXR signal. (b) Edge Mirnov Coil spectrogram. (c) Electron flux measured by divertor probes and Extreme Ultra-Violet (XUV) rotation in divertor region (d) Edge high-frequency magnetic perturbations and core FN signal.

5. FAST PARTICLE ACCELERATION NEAR TI-ITB REGION

TRANSP simulations predicted a distinct double-peaked energy structure, indicating a notable peak in the fast ion population at approximately 60 keV (as illustrated in Fig.6 (c)). As shown in Equation 1 of Ref.23, the injection energy of NBI is $E_0 = 60$ keV. Beam particles with energies of $E_0/2$ and $E_0/3$ are also injected during NBI heating, with a power ratio of E_0 : $E_0/3$ = 6:2:1. In shot #136377, due to the reduced plasma density, the collision rate decreased, and the beam fast ions were not fully thermalized. Therefore, the initial high-energy ion distribution calculated by NUBEAM exhibits a two-peaked structure, with the higher energy peak located near E_0 0 keV. The fast ion energy spectrum measured by the CVD diamond detector (Fig. 6 (a)) shows an increase in fast ion energy following Ar injection. Scattered neutron counts (Fig. 6 (b)) also increase. These increase reveals an acceleration of fast ions from energies below 1.3 MeV to over 1.3 MeV, might owing to extra collisional heating from more 2.45MeV neutrons [28] scattered by injected Ar. The inversion of neutron camera data reveals

three distinct fast ion distribution bands [29]. This spatial structure can be explained by the NBI deposition profile and plasma confinement properties. The initial NBI energy deposition is centered at ρ ~0.4. However, strong pressure gradients, typically present at ρ ~0.25 and ρ ~0.9 during most NBI discharges, act to effectively confine fast ions at these two locations. Notably, the third band at ρ ~0.7 is absent prior to Ar injection. The emergence of fast ions in this region is therefore a direct consequence of the Ar seeding. The neutron distribution predicted by NUBEAM is concentrated within ρ ~ 0.4 (Fig. 6-e), consistent with the neutron camera measurement (Fig. 6-d) which is dominated by uncollided neutrons. Additionally, the fast ion density in the core reaches 5×10^{18} m⁻³, which is ~16% of the core electron density.

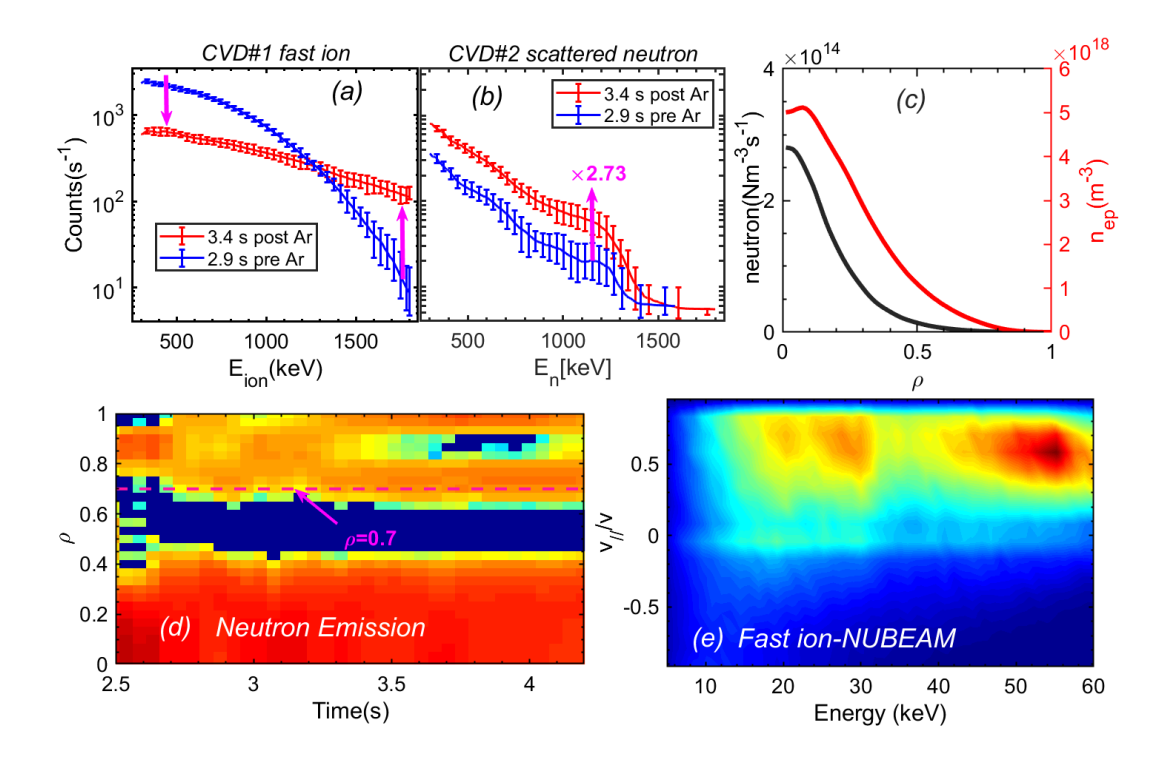


Fig. 6 Fast Ion Dynamics. (a) Neutralized fast ion energy spectra measured by a CVD#1 diamond detector (see Appendix A). (b) Scattered neutron energy spectra by another CVD#2. (c) NUBEAM predicated neutron and fast ion density profile, $\frac{n_{ep,0}}{n_{e0}} \sim 16\%$. (d) Radial neutron emission (log. Scale) measured by neutron camera [29]. (e) Fast ion pitch angle distribution from NUBEAM simulation. The neutron yield calculated by NUBEAM is $2.0 \times 10^{14} n/s$.

Fast electron dynamics were monitored using the HXR diagnostic [12, 30]. As depicted in Fig. 7, Ar injection triggered bursts of fast electrons near $\rho\sim0.4$. Furthermore, NBI injection resulted in off-axis peaked features in the FE profile. Panels (b) and (c) of Fig. 7 specifically show the bursting of fast electrons (within the 40-80 keV energy range) near $\rho\sim0.4$. Significantly, the emergence of these fast electrons coincides spatially with the second peak in neutron emission observed in Fig. 6 (d).

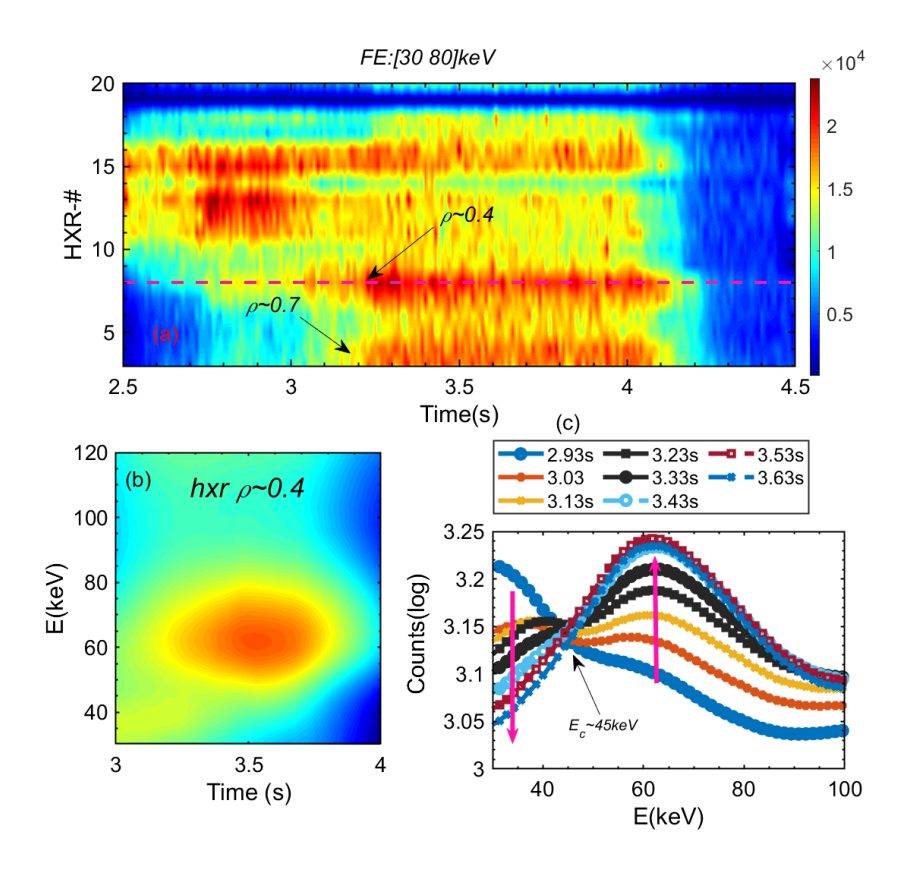


Fig. 7 Fast electron dynamics after Ar injection. (a) contour plot of FE with E= [30 80] keV. (b) FE energy spectrum evolution near $\rho \sim 0.4$. (c) FE spectrum at t=3.5s ($\rho \sim 0.4$).

In conclusion, on the EAST tokamak, we achieved low-collisionality conditions with high Ti, mimicking scenarios anticipated in future fusion reactors employing vertically directed NBI. In the Ti peak region, we observed multi-scale instabilities, including BAE, FB, LLM, and ion-scale turbulence. Notably, LLM activity induces core current redistribution. Furthermore, the coexistence of LLM and FB reduces the amplitude of ITG turbulence. Following the injection of Ar impurities, we observed a bursting event of the fast electron near ρ ~0.4. LLM, characterized by weak magnetic shear, exhibits an inherent multi-scale nature, with harmonics extending to n>18. A core-edge coupling process was clearly identified during the Ti-ITB dithering phase, where the n=0 low-frequency mode plays a critical role in mediating this coupling and mitigating fast ion loss.

6. REFERENCES

- [1] X. Du, et al., Phys. Rev. Letts. 127 (2021) 025001
- [2] A. Fasoli Phys. Rev. Letts. 130 (2023) 220001
- [3] S. Jardin, et al., 2015 Phys. Rev. Lett. 115 215001
- [4] Lorenzini R. et al 2009 Nat. Phys. 5 570
- [5] Menard J. et al 2006 Phys. Rev. Lett. 97 095002
- [6] L. Xu, et al., Nucl. Fusion 64 (2024) 046024
- [7] G. Brochard, et al., 2024 Phys. Rev. Lett. 132 075101

- [8] W. Mao, et al., Phys. Rev. Res. 5 (2023) L022047
- [9] S. Wang, et al., 2024 Phys. Rev. Lett. 132 065106
- [10] X Yang, et al., Nucl. Fusion 64 (2024) 016030
- [11] J. Qian, et al. Nucl. Fusion 57 (2017) 036008
- [12] R. Zhou, et al., Fusion Eng. and Des. 205 (2024) 114548
- [13] K. Chen, et al., Rev. Sci. Instrum. 87 (2016) 063504
- [14] Y. Liu, et al., Fusion Eng. and Des. 136 (2018) 72
- [15] G. Li et al., Plasma Phys. Control. Fusion 55 (2013) 125008
- [16] G. Zhong, et al., Plasma Phys. Control. Fusion 58 (2016) 075013
- [17] T Zhang, et al., Plasma Phys. Control. Fusion 59 (2017) 065012
- [18] Q. Zang, et al., Plasma Sci. Technol. 12 (2010) 144
- [19] Y. Shi, et al., Phys. Control. Fusion 52 (2010) 085014
- [20] L. Xu, et al., 2015 Phys. Plasma 22 122510
- [21] W. Shen, et al., 2025 Nucl. Fusion 65 066012
- [22] L. Xu, et al., 2021 Nucl. Fusion 61 076005
- [23] W. Shen, et al., 2017 Nucl. Fusion 57 11035
- [24] Y. Yuan, et al., 2020 Nucl. Fusion 60 016003
- [25] K. Geng, et al., 2024 Nucl. Fusion 64 056017
- [26] N. Pu et al. 2015 JINST 10 P12013
- [27] H. Wang, et al., 2014 Nucl. Fusion 54 124001
- [28] S. Lin, et al., 2024 JINST 19 P07017
- [29] Y. Zhang, et al., Fusion Eng. and Des. 206 (2024) 114602
- [30] Y. Chao, et al., Nucl. Fusion 64 (2024) 036015

Acknowledgments

This work was partly supported by the National Natural Science Foundation of China under grants 12375230 and 12275309. This work was also partly supported by the National Key R&D Program of China Grant Nos.2022YFE03010003.